



**HAL**  
open science

## Microstructural evolution in Al-Mn-Cu-(Be) alloys

Niko Rozman, Jozef Medved, Franc Zupanic

► **To cite this version:**

Niko Rozman, Jozef Medved, Franc Zupanic. Microstructural evolution in Al-Mn-Cu-(Be) alloys. Philosophical Magazine, 2011, pp.1. 10.1080/14786435.2011.608733 . hal-00728899

**HAL Id: hal-00728899**

**<https://hal.science/hal-00728899>**

Submitted on 7 Sep 2012

**HAL** is a multi-disciplinary open access archive for the deposit and dissemination of scientific research documents, whether they are published or not. The documents may come from teaching and research institutions in France or abroad, or from public or private research centers.

L'archive ouverte pluridisciplinaire **HAL**, est destinée au dépôt et à la diffusion de documents scientifiques de niveau recherche, publiés ou non, émanant des établissements d'enseignement et de recherche français ou étrangers, des laboratoires publics ou privés.



**Microstructural evolution in Al-Mn-Cu-(Be) alloys**

Journal:	<i>Philosophical Magazine &amp; Philosophical Magazine Letters</i>
Manuscript ID:	TPHM-11-Apr-0154.R1
Journal Selection:	Philosophical Magazine
Date Submitted by the Author:	16-Jul-2011
Complete List of Authors:	Rozman, Niko; University of Maribor, Faculty of Mechanical Engineering Medved, Jozef; University of Ljubljana, Faculty of Natural Sciences and Engineering Zupanic, Franc; University of Maribor, Faculty of Mechanical Engineering
Keywords:	aluminium alloys, quasicrystalline alloys, microstructure, microhardness
Keywords (user supplied):	

SCHOLARONE™  
Manuscripts

## Microstructural evolution in Al-Mn-Cu-(Be) alloys

Niko Rozman<sup>1</sup>, Jožef Medved<sup>2</sup>, Franc Zupanič<sup>1</sup>

*University of Maribor, Faculty of mechanical engineering, Maribor, Slovenia*

*University in Ljubljana, Faculty of Natural Sciences and Engineering, Slovenia*

Corresponding author  
Franc Zupanič  
University of Maribor  
Faculty of Mechanical Engineering  
Smetanova 17  
SI-2000 Maribor  
Slovenia  
tel. +386 2 220 7863  
fax. +386 2 220 7990  
e-mail: [franc.zupanic@uni-mb.si](mailto:franc.zupanic@uni-mb.si)

Peer Review Only

## Microstructural evolution in Al-Mn-Cu-(Be) alloys

This article investigates the effects of alloying elements on the microstructural evolution of Al-rich Al-Mn-Cu-(Be) alloys during solidification, and subsequent heating and annealing. The samples were characterized using scanning electron microscopy, energy dispersive X-ray spectroscopy, synchrotron X-ray diffraction, time-of-flight secondary-ion mass spectroscopy, and differential scanning calorimetry. In the ternary  $\text{Al}_{94}\text{Mn}_3\text{Cu}_3$  (at. %) alloy, the phases formed during slower cooling ( $\approx 1 \text{ K s}^{-1}$ ) can be predicted by the known Al-Mn-Cu phase diagram. The addition of Be prevented the formation of  $\text{Al}_6\text{Mn}$ , decreased the fraction of  $\tau_1\text{-Al}_{29}\text{Mn}_6\text{Cu}_4$ , and increased the fraction of  $\text{Al}_4\text{Mn}$ . During faster cooling ( $\approx 1000 \text{ K s}^{-1}$ ),  $\text{Al}_4\text{Mn}$  predominantly formed in the ternary alloy, whereas in the quaternary alloys the icosahedral quasicrystalline phase dominated. Further heating and annealing of the alloys caused an increase in the volume fractions of  $\tau_1$  in all alloys, and  $\text{Be}_4\text{Al}(\text{Mn,Cu})$  in quaternary alloys, while fractions of all other intermetallic phases decreased. Solidification with a moderate cooling rate ( $\approx 1000 \text{ K s}^{-1}$ ) caused considerable strengthening, which was reduced by annealing for up to 25 % in the quaternary alloys, while hardness remained almost the same in the ternary alloy.

Keywords: aluminium; quasicrystal; microstructure; beryllium

### 1 Introduction

Modern engineering materials must be able to carry high load and simultaneously possess high reliability. The materials of choice have high-strength, high-toughness, and low density. From among them, aluminium alloys still play an important role, in spite of the rapid development of lighter magnesium alloys and different types of lightweight composites. Al-casting alloys have been used successfully in many applications in the automotive and aerospace industries. The most versatile Al-Si alloys can attain a very wide range of properties, the strongest ones e.g.  $\text{AlSi12CuNiMg}$ , can have tensile strengths as high as 400 MPa, and elongation of around 5 %.

1  
2  
3 Over the years, many attempts have been made to provide even stronger and more  
4 ductile alloys. Inoue and Kimura [1] produced several quasicrystalline strengthened Al-  
5 alloys using gas atomisation of the melt, followed by densification with warm extrusion  
6 or pressing. Among these alloys, the alloys arising from the Al-Mn-Cu system  
7 possessed comparable strength to commercial high-strength aluminium alloys (500-600  
8 MPa), and much better ductility (elongation > 20 %). In these alloys, appropriate  
9 properties were achieved by rapid solidification, but not when applying moderate  
10 cooling rates. To date several new Al-casting alloys strengthened by the quasicrystalline  
11 phase have been developed. However, in most cases, besides the quasicrystalline phase  
12 several additional intermetallic phases have also been found, adversely affecting  
13 ductility [2-4]. In addition, most of these alloys possessed rather high liquidus  
14 temperatures exceeding 800 °C, which may be inconvenient for aluminium foundries.

15  
16  
17  
18  
19  
20  
21  
22  
23  
24  
25  
26  
27  
28  
29  
30  
31  
32 Recently an  $\text{Al}_{94}\text{Mn}_2\text{Cu}_2\text{Be}_2$  alloy was developed possessing mainly i-phase in the Al-  
33 rich solid solution matrix ( $\alpha\text{-Al}$ ). This i-phase was formed at moderate cooling rates  
34 typical for conventional die-casting, the liquidus temperature of the alloy being below  
35 700 °C [5]. Previous investigations have shown that (1) Mn is a transition element  
36 enabling the formation of metastable quasicrystals [6], Be reduces critical cooling rate  
37 for quasicrystal formation [3], while Cu can stabilize i-phase [7], enable strengthening  
38 by precipitation hardening, and reduce the liquidus temperature [8]. However, in order  
39 to exploit the potential of the Al-Mn-Cu-Be alloy system to the greatest extent, it is  
40 necessary to determine the effect of alloying elements and processing conditions on the  
41 microstructural evolution and mechanical properties, in a more systematic way.  
42  
43  
44  
45  
46  
47  
48  
49  
50  
51  
52  
53  
54  
55  
56  
57  
58  
59  
60

## 2 Materials and methods

Four alloys were investigated during this study, and their chemical compositions are given in Table 1. The content of Al in each alloy was above 92 at. % in order to provide large fraction of though aluminium solid solution. Be-content was varied with the aim to obtain information whether quasicrystalline phase may form even at very small amounts of beryllium. Different Mn-contents were selected to influence the fractions of intermetallic phases, and consequently the final mechanical properties. The alloys were prepared from pure Al 99.9, and AlBe5.5, AlMn20 and AlCu50 master alloys using vacuum-induction melting. Thereafter, they were die-cast into a cylindrical copper die with a diameter of 50 mm (approximate cooling rate was few  $\text{K s}^{-1}$ ), and into a smaller copper die with dimensions 100 mm  $\times$  10 mm  $\times$  1 mm (approximate cooling rate was  $1000 \text{ K s}^{-1}$ ). The samples were investigated using a SEM (Sirion 400 NC, FEI) equipped with EDS (Inca 350, Oxford Instruments), XRD (synchrotron radiation,  $\lambda = 0.99598 \text{ nm}$ , Sincrotrone Elettra, Trieste, Italy), and ToF SIMS (Time-of-Flight Secondary Ion-Mass Spectroscopy, Cameca TOF-IV). The samples for transmission electron microscopy TEM (Titan 80-300, FEI) were prepared using focussed ion beam technique (Helios Nanolab, FEI). The indentation hardness tests were carried out on a Fisherscope H100C testing machine (Fisher Technology). The loading and unloading times were 10 seconds each. The maximum load applied was 1 N. The results were evaluated using EN-standard [9]. Differential scanning calorimetry (DSC) was performed in an STA 449 Jupiter between  $100 \text{ }^\circ\text{C}$  and  $1100 \text{ }^\circ\text{C}$ , with heating and cooling rates of  $20 \text{ K min}^{-1}$  in a nitrogen atmosphere.

### 3 Results

#### 3.1 Microstructural characterization

##### 3.1.1 Slow-cooling

Figure 1 shows backscattered electron micrographs of all alloys after casting into a larger die. Each alloy contained several phases. The phases labelled in the micrographs were identified using Z-contrast analysis [10], XRD (Fig. 2), EDS-results and ToF SIMS (Fig. 3). The phases were rather coarse with sizes up to a few hundred microns. The microstructure of the ternary alloy  $\text{Al}_{94}\text{Mn}_3\text{Cu}_3$  was composed of Al-rich solid solution ( $\alpha$ -Al), and four intermetallics:  $\text{Al}_4\text{Mn}$ ,  $\text{Al}_6\text{Mn}$ ,  $\tau_1$  ( $\text{Al}_{29}\text{Mn}_6\text{Cu}_4$ ) and  $\theta$ - $\text{Al}_2\text{Cu}$ .  $\text{Al}_4\text{Mn}$  was mainly surrounded by  $\text{Al}_6\text{Mn}$ , while  $\text{Al}_6\text{Mn}$  was surrounded by  $\tau_1$ .  $\theta$ - $\text{Al}_2\text{Cu}$  was present at the sites where solidification had terminated. Such distribution of phases strongly indicates that the solidification followed a sequence of reactions in the ternary Al-Mn-Cu phase diagram. However, the binary peritectic reaction ( $\text{L} + \text{Al}_4\text{Mn} \rightarrow \text{Al}_6\text{Mn}$ ) and the ternary transition reaction ( $\text{L} + \text{Al}_6\text{Mn} \rightarrow \tau_1 + \alpha$ -Al) did not move on to completion due to non-equilibrium solidification conditions. Thus, in this alloy,  $\text{Al}_4\text{Mn}$  and  $\text{Al}_6\text{Mn}$  remained in the microstructure at room temperature besides the equilibrium phases:  $\tau_1$ ,  $\theta$ - $\text{Al}_2\text{Cu}$  and  $\alpha$ -Al. The peaks of the equilibrium phases dominated in the XRD-spectra, while the peaks of the minor phases  $\text{Al}_4\text{Mn}$  and  $\text{Al}_6\text{Mn}$  were often superimposed by other peaks (Fig. 2). It should be noted that  $\text{Al}_4\text{Mn}$ ,  $\tau_1$ , and  $\text{Al}_6\text{Mn}$  possess rather large unit cells [8]. Consequently, they can be more easily identified at lower angles, while at higher angles their peaks overlap with other peaks. The lattice parameters of the present phases were:  $a = 0.4029 \pm 0.0010$  nm for FCC  $\alpha$ -Al;  $a = 0.6049 \pm 0.0015$  nm and  $c = 0.4857 \pm 0.0007$  nm for tetragonal  $\theta$ - $\text{Al}_2\text{Cu}$  (0.3 % different in comparison to PDF 89-1981);  $a = 2.4113 \pm 0.0090$  nm,  $b = 0.7724 \pm 0.0040$

1  
2  
3 nm and  $c = 1.2506 \pm 0.0030$  nm for orthogonal  $\tau_1$ (; and  $a = 0.7523 \pm 0.0040$  nm,  $b =$   
4  
5  
6  $0.6496 \pm 0.0050$ ,  $c = 0.8831 \pm 0.0045$  for orthogonal  $\text{Al}_6\text{Mn}$ , whereas it was not  
7  
8 possible to reliably determine the lattice parameters of hexagonal  $\text{Al}_4\text{Mn}$  due to its very  
9  
10 small volume fraction. The lattice parameters of  $\Theta\text{-Al}_2\text{Cu}$ ,  $\tau_1$  and  $\text{Al}_6\text{Mn}$  was almost the  
11  
12 same as in the corresponding PDF-files. The lattice parameter of  $\alpha\text{-Al}$  was  
13  
14 approximately 1.5 % smaller than that of pure Al, presumably due to smaller atomic  
15  
16 radii of substitutional Cu and Mn atoms.  
17

18  
19  
20 The addition of Be brought some important microstructural changes:

- 21 •  $\text{Al}_6\text{Mn}$  was absent in the quaternary alloys.
- 22 • The fraction of  $\text{Al}_4\text{Mn}$  became larger, especially in the alloy  
23  
24  $\text{Al}_{92.4}\text{Mn}_{4.4}\text{Cu}_{1.6}\text{Be}_{1.6}$  containing the highest Mn-content. The lattice parameters  
25  
26 of hexagonal  $\text{Al}_4\text{Mn}$  were:  $a = 1.9958 \pm 0.0170$  and  $c = 2.4711 \text{ nm} \pm 0080 \text{ nm}$ ,  
27  
28 which was almost identical to the published values.  
29  
30
- 31 • The fraction of  $\tau_1$  became smaller, and its lattice parameters were impossible to  
32  
33 determine reliably. It was predominantly present in the form of a thin layer  
34  
35 around the  $\text{Al}_4\text{Mn}$ -particles, as well in the regions where solidification had  
36  
37 ended.  
38  
39
- 40 • A Be-rich phase occurred that presumably formed during the terminal stages of  
41  
42 solidification.  
43  
44  
45  
46  
47  
48  
49

50  
51 In most phases, the analysis of Be normally presents a problem because a phase must  
52  
53 contain a very high Be-content to be detected using EDS. However, Be-rich phases can  
54  
55 be recognized in the backscattered electron micrographs based on their Z-contrast.  
56  
57 These phases are much darker than would be expected according to their chemical  
58  
59 composition obtained using EDS because when using EDS, only the contents of Al, Mn  
60

1  
2  
3 and Cu could be determined [10]. It was discovered that in all Be-rich particles, the  
4  
5 sums of Cu- and Mn-content as atomic percentages were equal to the Al-contents. This  
6  
7 suggested that the possible Be-phase was  $\text{Be}_4\text{Al}(\text{Mn},\text{Cu})$ , and not a Raynor phase  
8  
9  $\text{Al}_{15}\text{Mn}_3\text{Be}_2$  [11]. This was also confirmed by XRD-results, which revealed that the  
10  
11 lattice parameter of  $\text{Be}_4\text{Al}(\text{Mn},\text{Cu})$  was close to that of pure cubic  $\text{Be}_4\text{AlMn}$  ( $a = 0.6110$   
12  
13  $\pm 0.0010$  nm). Thus Cu can partly substitute Mn in  $\text{Be}_4\text{AlMn}$ , which was also found for  
14  
15 Ni [12]. On the other hand, Fleury et al. [13] found that Si can replace both Mn and Al  
16  
17 in  $\text{Be}_4\text{AlMn}$ .  $\text{Be}_4\text{AlMn}$  can also represent a very suitable heterogeneous nucleation site  
18  
19 for the  $\text{i}$ -phase [13, 14]. In the investigated alloys  $\text{Be}_4\text{Al}(\text{Mn},\text{Cu})$  emerged during the  
20  
21 terminal stages of solidification, whereas it appeared at the beginning of solidification in  
22  
23  $\text{Al}_{94}\text{Mn}_2\text{Cu}_2\text{Be}_2$  [5].  
24  
25  
26  
27  
28  
29

30 Fig. 3 shows ToF SIMS mapping of Al-, Cu-, Be-, and Mn-ions. It is clear that Be is not  
31  
32 only in the Be-rich phase  $\text{Be}_4\text{Al}(\text{Mn},\text{Cu})$ , but also in  $\tau_1$ ,  $\text{Al}_4\text{Mn}$  and  $\theta\text{-Al}_2\text{Cu}$ . However,  
33  
34 the content of Be must be rather small, in the order of a few atomic percentages. There  
35  
36 is almost no Be in the Al-rich solid solution, which is consistent with its very low  
37  
38 maximum solubility in Al [15].  
39  
40  
41  
42

43 Fig. 4 shows DSC-cooling curves. All curves clearly show three peaks, despite the fact,  
44  
45 that even during solidification of the ternary alloy, many more processes should take  
46  
47 place [8]. However, other peaks cannot be seen due to overlapping with the main peaks.  
48  
49

50 The DSC-heating curves were qualitatively the same, indicating the appearance of the  
51  
52 same reactions during heating and cooling. It is important that the liquidus temperature  
53  
54 stayed below  $740^\circ\text{C}$ , even for the alloy  $\text{Al}_{92.4}\text{Mn}_{4.4}\text{Cu}_{1.6}\text{Be}_{1.6}$  containing the highest  
55  
56 cumulative amount of Be and Mn. This is still appropriate for the practical applications  
57  
58 of these alloys in Al-foundries. The previously investigated alloy  $\text{Al}_{94}\text{Mn}_2\text{Be}_2\text{Cu}_2$  [5],  
59  
60

1  
2  
3 possessed the liquidus temperature below 700 °C, and the alloy  $\text{Al}_{95.4}\text{Mn}_{1.8}\text{Cu}_{1.5}\text{Be}_{1.3}$   
4  
5 with somewhat lower amounts of alloying elements had even as low liquidus  
6  
7 temperature as 655 °C. Based on the comparison of DSC-traces with the backscattered  
8  
9 electron micrographs in Fig. 1, it is possible to predict the main processes taking place  
10  
11 on the appearance of peaks. Peaks denoted with 1 indicate the beginning of primary  
12  
13 solidification when  $\text{Al}_4\text{Mn}$  starts to form ( $\text{L} \rightarrow \text{Al}_4\text{Mn}$ ), peaks denoted by 2 indicate the  
14  
15 formation of  $\alpha\text{-Al}$  (perhaps via the transition reaction  $\text{L} + \text{Al}_4\text{Mn} \rightarrow \alpha\text{-Al} + \tau_1$ ), whilst  
16  
17 peaks 3 indicate the occurrence of the last stages of solidification, when  $\theta\text{-Al}_2\text{Cu}$  and  
18  
19  $\text{Be}_4\text{Al}(\text{Mn,Cu})$  formed. In all four-component alloys, the starting temperatures of peaks  
20  
21 3 are similar to the temperature of the ternary eutectic reaction in the Al-Mn-Cu system:  
22  
23  $\text{L} \rightarrow \alpha\text{-Al} + \theta\text{-Al}_2\text{Cu} + \tau_1$ . In four component alloys, microstructural investigation  
24  
25 indicates that even four phases ( $\alpha\text{-Al} + \tau_1 + \theta\text{-Al}_2\text{Cu} + \text{Be}_4\text{Al}(\text{Mn,Cu})$ ) were present in  
26  
27 larger interdendritic spaces (Fig. 1c).  
28  
29  
30  
31  
32  
33  
34  
35

### 3.1.2 Moderate-cooling

36  
37  
38 Fig. 5 shows backscattered electron micrographs of the investigated alloys after casting  
39  
40 in a small copper die, and Fig. 6 their corresponding X-ray diffraction patterns. There  
41  
42 are profound differences in the microstructures and phase compositions compared to the  
43  
44 samples cooled at the lower cooling rates (Figs. 1 and 2). In all alloys, except in the  
45  
46 ternary, large intermetallic phases were eliminated. In the  $\text{Al}_{94}\text{Mn}_3\text{Cu}_3$  alloy, primary  
47  
48  $\text{Al}_4\text{Mn}$  particles were present in the microstructure, however their sizes were within the  
49  
50 range of only 5–10  $\mu\text{m}$ , only occasionally  $\text{Al}_6\text{Mn}$  was found. Small fractions of  $\tau_1$  and  
51  
52  $\theta\text{-Al}_2\text{Cu}$  were merely found in the interdendritic spaces. Be also had an important effect  
53  
54 on microstructural evolution at higher cooling rates. The icosahedral quasicrystalline  
55  
56 phase formed in all Be-bearing alloys, in contrast to the ternary  $\text{Al}_{94}\text{Mn}_3\text{Cu}_3$  alloy. This  
57  
58  
59  
60

1  
2  
3 can either be a part of a two-phase heterogeneous structure, which can be called binary  
4 eutectic, consisting of an  $\alpha$ -Al and lamellar i-phase (Fig. 5a-c) or as a primary i-phase in  
5 the form of a petal-like particles or well developed dendrite (Fig. 5d).  
6  
7  
8  
9

10  
11 Primary i-phase dendrites were very frequent in  $\text{Al}_{92.4}\text{Mn}_{4.4}\text{Cu}_{1.6}\text{Be}_{1.6}$  having the highest  
12 Mn-content, whereas they were encountered only occasionally in  $\text{Al}_{96.5}\text{Mn}_{1.3}\text{Cu}_{1.6}\text{Be}_{0.6}$   
13 and  $\text{Al}_{95.4}\text{Mn}_{1.8}\text{Cu}_{1.5}\text{Be}_{1.3}$ . The fraction of the binary eutectic increased along with the  
14 higher Be- and Mn-contents.  $\theta$ - $\text{Al}_2\text{Cu}$  can be found in the interdendritic spaces of all  
15 alloys, and its peaks are rather pronounced in XRD-spectra (Fig. 6). In addition, another  
16 phase, presumably  $\text{Al}_4\text{Mn}$ , envelopes the ( $\alpha$ -Al + i-phase) cells in  $\text{Al}_{92.4}\text{Mn}_{4.4}\text{Cu}_{1.6}\text{Be}_{1.6}$   
17 (Fig. 5d), and its peaks can be found in the XRD-trace (Fig. 6). The peaks of i-phase  
18 were rather broad, and often shifted from their ideal positions, indicating the presence of  
19 large phason strains. The presence of i-phase was further confirmed using TEM. Fig. 7a  
20 shows few branches of the eutectic i-phase. Its selected area diffraction pattern taken  
21 along a fivefold direction revealed clearly its quasiperiodic nature (Fig. 7b). Twofold  
22 diffraction pattern allowed us to determine its quasilattice constant that was found to be  
23 0,46 nm, which is the same as in the binary Al-Mn alloy. The lattice parameters of other  
24 phases present in moderately cooled samples did not differ much from the lattice  
25 parameters of the same phases in the slowly cooled samples.  
26  
27  
28  
29  
30  
31  
32  
33  
34  
35  
36  
37  
38  
39  
40  
41  
42  
43  
44  
45  
46  
47

48 Be was concentrated in the i-phase (Fig. 8) because no other Be-rich phase; e.g.  
49  $\text{Be}_4\text{Al}(\text{Mn},\text{Cu})$  was present. This means, that the i-phase can dissolve considerable  
50 amounts of Be, which makes it more stable. This was suggested by Song et al. [3], and  
51 experimentally confirmed by using AES for the i-phase in the Al-Mn-Be [16] and Al-  
52 Mn-Be-Si [13] alloys.  
53  
54  
55  
56  
57  
58  
59  
60

### 3.1.3 Heating and annealing

The samples cast into the smaller die were exposed to uniform heating of  $20 \text{ K min}^{-1}$  up to  $600 \text{ }^\circ\text{C}$ , which is slightly above the solidus temperatures of all alloys. The resulting DSC-traces are depicted in Fig. 9. The ternary alloy exhibited a larger exothermic peak starting at approximate  $500 \text{ }^\circ\text{C}$  (denoted by 2). As the beryllium content increases, this peak grows smaller, and in the alloy  $\text{Al}_{92.4}\text{Mn}_{4.4}\text{Cu}_{1.6}\text{Be}_{1.6}$  it can hardly be observed. On the other hand, a peak denoted with 1 started to appear by the addition of Be. These results suggest that the initial microstructure becomes unstable above  $400 \text{ }^\circ\text{C}$  for four-component alloys, whereas decomposition of microstructure begins above  $500 \text{ }^\circ\text{C}$  in the ternary alloy.

Figs. 10 and 11 clearly point to some variations in microstructures and phase compositions compared to the as-cast condition. The most striking effect is the appearance of  $\tau_1$ -peaks in all alloys, and its lattice parameters were apparently identical to those published in Ref. 8. Phase  $\tau_1$  almost completely replaces  $\text{Al}_4\text{Mn}$  in the ternary alloy, and in addition,  $\tau_1$ -particles precipitate from the solid solution. In the quaternary alloys, most of  $i$ -phase was preserved. The shapes of the primary  $i$ -phase particles remained almost unchanged, however their surfaces became decorated with  $\tau_1$  and  $\text{Be}_4\text{Al}(\text{Mn,Cu})$  particles. The morphology of the eutectic  $i$ -phase changed completely, namely, branched rods transformed into faceted particles with diameters of  $500\text{--}1000 \text{ nm}$ . A similar transition was found in our previous work [5]. Most of the  $\theta\text{-Al}_2\text{Cu}$  phase present in the as-cast condition dissolved to a rather large extent. Needle-like precipitates appeared within  $\alpha\text{-Al}$  with lengths from  $1$  to  $2 \text{ }\mu\text{m}$  and a diameter of  $100 \text{ nm}$ , their nature has not as yet been investigated in detail, but they might be  $\tau_1$ .

1  
2  
3 According to the results of microstructural analysis it is possible to state that the peak  
4  
5 on the DSC-curve of the ternary alloy arises from the precipitation of  $\tau_1$  in the matrix  
6  
7 and transformation of  $\tau_1$  into  $\text{Al}_4\text{Mn}$ . In the quaternary alloys, the first peak can be  
8  
9 attributed to the precipitation of  $\tau_1$  in the  $\alpha$ -Al matrix, while the second peak can be  
10  
11 assigned to the transformation of i-phase into  $\tau_1$  and  $\text{Be}_4\text{Al}(\text{Mn,Cu})$ , which definitely  
12  
13 occurred at temperatures above 500 °C, since most of the i-phase was preserved during  
14  
15 annealing at 500 °C.  
16  
17  
18  
19  
20  
21

### 22 ***3.2 Microstructural evolution upon solidification***

23  
24 The presented results clearly show the strong effects of cooling rate and chemical  
25  
26 composition on microstructural evolution in Al-Mn-Cu-(Be) alloys during processing.  
27  
28 In the Al-rich corner of the Al-Mn-Cu system, the Mn:Cu ratio has a decisive role in  
29  
30 determining equilibrium phases [8], when additions of Cu and Mn exceed their  
31  
32 solubility limits in Al. The critical ratio amounts 3:2, when only  $\alpha$ -Al and  $\tau_1$  are in the  
33  
34 equilibrium. When this ratio is higher than 3:2, then the equilibrium phases are  $\alpha$ -Al,  
35  
36  $\text{Al}_6\text{Mn}$  and  $\tau_1$ , whereas when this ratio is smaller than 3:2, then  $\alpha$ -Al,  $\theta$ - $\text{Al}_2\text{Cu}$  and  $\tau_1$   
37  
38 are the equilibrium phases, such in the case of the investigated  $\text{Al}_{94}\text{Mn}_3\text{Cu}_3$  alloy.  
39  
40  
41  
42  
43  
44

45 Even during slow-cooling, all five phases are present near the Al-rich corner of the  
46  
47 ternary Al-Cu-Mn system formed upon solidification. This is unsurprising because  
48  
49 solidification is an inherently non-equilibrium process, linked with spatial and temporal  
50  
51 varying temperature and compositional fields. The non-equilibrium phases  $\text{Al}_4\text{Mn}$  and  
52  
53  $\text{Al}_6\text{Mn}$  were formed during the initial stages of solidification and were not consumed  
54  
55 completely by the subsequent peritectic and transition reactions [8]. Nevertheless, at  
56  
57 least local solidification conditions did not strongly deviate from the equilibrium  
58  
59 conditions. On the other hand, a faster cooling rate strongly influenced the nucleation  
60

1  
2  
3 and growth of phases. It completely suppressed the formation of  $Al_6Mn$  and partly  $\tau_1$ ,  
4  
5 but strongly enhanced the formation and growth of  $Al_4Mn$ . It should be remembered  
6  
7 that the equilibrium phase in the Al-Mn phase diagram,  $\mu-Al_4Mn$  [17], and other  
8  
9 strongly related Al-Mn intermetallic phases [14, 18], possess very large unit cells, and  
10  
11 icosahedral-cluster substructures. Thus, the cluster substructure existing in the  
12  
13 supercooled melt [19], which is achieved by higher cooling rates, can facilitate the  
14  
15 formation of such phases.  
16  
17  
18  
19

20  
21 Additions of Be to Al-Mn-Cu alloys promote the formation of  $Al_4Mn$  even at slow  
22  
23 cooling rates, whereas the icosahedral phase forms at higher-cooling rates only. Both  
24  
25 phases are characterized by the icosahedral cluster substructure. This strongly suggests  
26  
27 that the Be-addition strengthens the icosahedral local order in the melt, as previously  
28  
29 proposed by Song et al. [3]. Upon slow cooling, only a low supercooling of the melt is  
30  
31 attained. Under such conditions, icosahedral clusters can arrange themselves in a  
32  
33 periodic way and  $Al_4Mn$  forms. However, at higher supercooling the growth rate  
34  
35 increases and clusters can only arrange themselves in a quasiperiodic way.  
36  
37  
38  
39

40  
41 Be-additions completely prevent the formation of  $Al_6Mn$  on solidification. This can be  
42  
43 based on kinetic or perhaps even thermodynamic reasons. In the latter case, the relative  
44  
45 stability of  $Al_4Mn$  relative to  $Al_6Mn$  is increased. This can enlarge the primary  
46  
47 solidification field for  $Al_4Mn$  compared to that of  $Al_6Mn$ . Be addition and the increased  
48  
49 cooling rate also suppress the formation of  $\tau_1$ . This can be explained by the fact that  $\tau_1$   
50  
51 is a quasicrystalline approximant for a decagonal quasicrystal [20] and therefore, the  
52  
53 preferred icosahedral order in the melt may not be convenient for the formation of  $\tau_1$ .  
54  
55  
56  
57  
58  
59  
60

### 3.3 Microstructural evolution on heating and annealing

During annealing, the system wants to attain the equilibrium condition. In the case of the ternary alloy, it is  $\alpha$ -Al +  $\tau_1$  +  $\theta$ -Al<sub>2</sub>Cu. The results suggest that it occurs in two steps: (1) partial dissolution of  $\theta$ -Al<sub>2</sub>Cu and precipitation of  $\tau_1$ -phase from the solid solution, and (2) transformation of primary Al<sub>4</sub>Mn to  $\tau_1$ . It seems that the latter process takes place in-situ, resulting in the same shape of  $\tau_1$  as Al<sub>4</sub>Mn. Precipitates  $\tau_1$ , formed during the first step, obviously provide sufficient hardening effect to prevent any softening during annealing. The same effect was observed during the extruding of Al-Mn-Cu-Zr alloy [22].

The equilibrium phases in Al-Mn-Cu-Be are strongly affected by the ratio Mn : Cu = 3 : 2. For the alloys Al<sub>96.5</sub>Mn<sub>1.3</sub>Cu<sub>1.6</sub>Be<sub>0.6</sub> and Al<sub>95.4</sub>Mn<sub>1.8</sub>Cu<sub>1.5</sub>Be<sub>1.3</sub> (Mn : Cu < 3 : 2) the expected equilibrium phases are  $\tau_1$  +  $\theta$ -Al<sub>2</sub>Cu +  $\alpha$ -Al + Be<sub>4</sub>Al(Mn,Cu), and for Al<sub>92.4</sub>Mn<sub>4.4</sub>Cu<sub>1.6</sub>Be<sub>1.6</sub> (Mn : Cu > 3 : 2):  $\tau_1$  + Al<sub>4</sub>Mn +  $\alpha$ -Al + Be<sub>4</sub>Al(Mn,Cu). The Be<sub>4</sub>Al(Mn,Cu) appears because the Be-contents exceed the cumulative solubility of Be in  $\alpha$ -Al, Al<sub>4</sub>Mn,  $\tau_1$  and  $\theta$ -Al<sub>2</sub>Cu. It is also a two step process, precipitation of  $\tau_1$  in  $\alpha$ -Al, and transformation of  $\theta$ -phase to  $\tau_1$  + Be<sub>4</sub>Al(Mn,Cu). It seems that the latter process is rather sluggish, since most of  $\theta$ -phase remained in the microstructure after 1 h annealing at 500 °C. However, increasing the temperature above 500 °C triggered this transformation.

### 3.4 Microindentation and hardness measurements

Table 2 summarizes the results of microindentation and hardness measurements. It is evident that the lowest mechanical properties were exhibited by the slowly cooled samples. This can be attributed to the very coarse microstructure. Such microstructure

1  
2  
3 also caused rather large scattering of the results in these samples in comparison to other  
4  
5 two conditions. Nevertheless, all alloys were considerably strengthened compared to  
6  
7 pure aluminium ( $HV \approx 0.17$  GPa). In fact, if we take into account that tensile strength is  
8  
9 3.7-times higher than hardness, and then the tensile strength is within the range between  
10  
11 400 MPa and 500 MPa. This is twice higher than the tensile strengths of most Al-Si  
12  
13 alloys, and comparable to the strengths of the strongest Al-cast alloys. Strengthening is  
14  
15 probably achieved by combination of precipitation and dispersion hardening. All phases  
16  
17 are namely much harder than the Al-rich matrix [22]. The reduced elastic modulus is  
18  
19 comparable to that of pure aluminium; it is slightly increased only in the alloy  
20  
21  $Al_{92.4}Mn_{4.4}Cu_{1.6}Be_{1.6}$ . The low values for the fraction of elastic energy,  $\eta_{IT}$ , also indicate  
22  
23 the possibility of strong plastic deformation. Annealing at 500 °C caused a softening of  
24  
25 quaternary alloys for about 25 %, but it did not affect the hardness of the ternary alloys.  
26  
27 This can be attributed to the strengthening effect of  $\tau_1$  [21].  
28  
29  
30  
31  
32  
33

34  
35 It was discovered that it is possible to obtain much higher strengths of quasicrystal-  
36  
37 strengthened cast Al-alloys [2, 4], however, these alloys had reduced ductility, and also  
38  
39 rather high liquidus temperatures.  
40  
41  
42

43  
44 The optimal additions of alloying elements are required, in order to achieve appropriate  
45  
46 strength after solidification and to enable further strengthening with precipitation  
47  
48 hardening. Firstly, approximately 0.5–1 at. % Be is necessary for promoting the  
49  
50 formation of an i-phase during solidification. Secondly, for achieving sufficient volume  
51  
52 fractions of hardening phases, i.e. formation of i-phase and suppression of other  
53  
54 intermetallic phases during solidification, and  $\tau_1$  after annealing, the Mn-content should  
55  
56 be 3–3.5 at.% Mn. Thirdly, for facilitating appropriate precipitation hardening the  
57  
58 approximate Cu-content should for 2 at.% exceed the fraction of Cu bonded to  $\tau_1$  and  
59  
60

1  
2  
3  $\text{Be}_4\text{Al}(\text{Mn,Cu})$ :  $0.66 \times \text{at. \% Mn} + 0.25 \times \text{at. \% Be}$ ; that is ( $\approx 4\text{--}4.5 \text{ at. \% Cu}$ ). Such a  
4  
5  
6 composition will provide sufficient volume fraction of tough  $\alpha$ -Al and a liquidus  
7  
8 temperature in the range of  $700 \text{ }^\circ\text{C}$ , which is still acceptable for aluminium high-  
9  
10 pressure die-casting.  
11

#### 12 13 14 15 **4 Conclusions**

16  
17  
18 The results of this investigation can lead us to the following conclusions:  
19

- 20  
21 (1) Both the cooling rate and chemical compositions of the alloys in Al-rich Al-Mn-  
22  
23 Cu-(Be) alloys have profound effects on microstructural evolution.  
24  
25
- 26 (2) Faster cooling rate ( $\approx 1000 \text{ K s}^{-1}$ ) suppresses the formation of  $\text{Al}_6\text{Mn}$  and  $\tau_1$ , and  
27  
28 promotes the formation  $\text{Al}_4\text{Mn}$ . However, it cannot trigger the formation of an i-  
29  
30 phase in the ternary  $\text{Al}_9\text{Mn}_3\text{Cu}_3$  alloy.  
31  
32
- 33 (3) Be-additions prevent the formation of  $\text{Al}_6\text{Mn}$  even at slow cooling rates, and  
34  
35 facilitate the formation of an i-phase at higher cooling rates. A considerable effect  
36  
37 can be obtained with rather low additions ( $\approx 0.5 \text{ at. \% Be}$ )  
38  
39
- 40 (4) Heating and annealing of the alloys lead to the formation of stable  $\tau_1$ -phase and  
41  
42  $\text{Be}_4\text{Al}(\text{Mn,Cu})$ , partial or complete dissolution of  $\theta$ - $\text{Al}_2\text{Cu}$ , and to the  
43  
44 decomposition of metastable  $\text{Al}_4\text{Mn}$  and i-phase. A quasicrystalline i-phase  
45  
46 remained in the samples annealed for 1 hour at  $500 \text{ }^\circ\text{C}$ , yet the shapes of primary  
47  
48 i-phase particles changed, as well as eutectic rodlike i-phase.  
49  
50
- 51 (5) Solidification with a moderate cooling rate ( $\approx 1000 \text{ K s}^{-1}$ ) caused considerable  
52  
53 strengthening, which was reduced by annealing by up to 25 % in quaternary  
54  
55 alloys, while in the ternary alloy hardness remained almost the same.  
56  
57  
58  
59  
60

1  
2  
3 Acknowledgements. We would like to thank Dr. Tonica Bončina and Dr. Peter Panjan for their  
4 kind assistance during indentation measurements. Rok Šulek (UM FS) is acknowledged for the  
5 vacuum melting and casting of alloys. We acknowledge Elettra, Sincrotrone Trieste, and the  
6 European Commission for reimbursement under EU contract RII3-CT-2004-506008 (IA-SFS),  
7 proposal 20090314. This work was also supported by the European Commission – Research  
8 Infrastructure Action under the FP6 “European Integrated Activity of Excellence and  
9 Networking for Nano and Micro-Electronics Analysis”. Project Number “026134 (RI3)  
10 ANNA”. This work was partly financed from the research programme P2 - 0120, of the  
11 Slovenian Ministry of Higher Education and Science.  
12  
13  
14  
15  
16  
17  
18  
19  
20

## 21 5 References

- 22  
23 [1] A. Inoue, H. Kimura, High-strength Al-based alloys consisting mainly of  
24 nanoscale quasicrystalline or amorphous particles, in: Synthesis and Properties  
25 of Mechanically Alloyed and Nanocrystalline Materials, Pts 1 and 2 - Ismanam-  
26 96, 1997, p. 873.  
27  
28 [2] F. Schurack, J. Eckert, L. Schultz, *Acta Mater.*, 49 (2001) p. 1351.  
29  
30 [3] G.S. Song, E. Fleury, S.H. Kim, W.T. Kim, D.H. Kim, *J. Mater. Res.*, 17 (2002)  
31 p. 1671.  
32  
33 [4] I.H. Jun, J.M. Kim, K.T. Kim, W.J. Jung, *Mater. Sci. Eng. A-Struct. Mater.*  
34 *Prop. Microstruct. Process.*, 449 (2007) p. 979.  
35  
36 [5] F. Zupanic, T. Boncina, N. Rozman, I. Anzel, W. Grogger, C. Gspan, F. Hofer,  
37 B. Markoli, *Z. Kristall.*, 223 (2008) p. 735.  
38  
39 [6] D. Shechtman, I. Blech, D. Gratias, J.W. Cahn, *Physical Review Letters*, 53  
40 (1984) p. 1951.  
41  
42 [7] J.Q. Guo, A.P. Tsai, *J. Mater. Res.*, 16 (2001) p. 3038.  
43  
44 [8] H. L. Lukas, Aluminum - Copper – Manganese, in Ternary alloys: a  
45 comprehensive compendium of evaluated constitutional data and phase  
46 diagrams, G. Petzow and G. Effenberg, eds., Weinheim; Basel (Switzerland);  
47 Cambridge; New York, NY, VCH Verlagsgesellschaft mbH., p. 567.  
48  
49 [9] EN ISO 14577-1:2002 Metallic materials - Instrumented indentation test for  
50 hardness and materials parameters - Part 1: Test method, (2002).  
51  
52  
53  
54  
55  
56  
57  
58  
59  
60

- 1  
2  
3  
4  
5  
6  
7  
8  
9  
10  
11  
12  
13  
14  
15  
16  
17  
18  
19  
20  
21  
22  
23  
24  
25  
26  
27  
28  
29  
30  
31  
32  
33  
34  
35  
36  
37  
38  
39  
40  
41  
42  
43  
44  
45  
46  
47  
48  
49  
50  
51  
52  
53  
54  
55  
56  
57  
58  
59  
60
- [10] F. Zupanic, *Mater. Charact.*, 61 (2010) p. 1335.
- [11] G.V. Raynor, C.R. Faulkner, J.D. Noden, A.R. Harding, *Acta Metall.*, 1 (1953) p. 629.
- [12] Aluminum-Beryllium-Manganese System, in *Aluminum alloys, Structure and Properties*, L.F. Mondolfo, ed., London, Boston, Sydney, Wellington, Durban, Toronto, Butterworths-London, 1976, p. 447.
- [13] E. Fleury, H.J. Chang, D.H. Kim, *Philos. Mag.*, 86 (2006) p. 349.
- [14] T. Boncina, B. Markoli, F. Zupanic, *J. Microsc.-Oxf.*, 233 (2009) p. 364.
- [15] J. Murray, D. Kahan, Al-Be (Aluminum-Beryllium), in: *Binary Alloy Phase Diagrams*, T. Massalski, ed., ASM International, 1990, p. 125.
- [16] F. Zupanic, T. Boncina, A. Krizman, W. Grogger, C. Gspan, B. Markoli, S. Spaic, *J. Alloy. Compd.*, 452 (2008) p. 343-347.
- [17] C.B. Shoemaker, D.A. Keszler, D.P. Shoemaker, *Acta Crystallogr. Sect. B-Struct. Commun.*, 45 (1989) p. 13.
- [18] S.H. Kim, G.S. Song, E. Fleury, K. Chattopadhyay, W.T. Kim, D.H. Kim, *Phil. Mag. A*, 82 (2002) p. 1495.
- [19] M.W. Chen, I. Dutta, T. Zhang, A. Inoue, T. Sakurai, *Appl. Phys. Lett.*, 79 (2001) p. 42.
- [20] X.Z. Li, K.H. Kuo, *Philos. Mag. B-Phys. Condens. Matter Stat. Mech. Electron. Opt. Magn. Prop.*, 66 (1992) p. 117.
- [21] H. Adachi, W. Itaka, T. Aida, K. Osamura, M. Imaoka, J. Kusui, *Trans. Indian Inst. Met.*, 62 (2009) p. 163.
- [22] T. Boncina, M. Cekada, B. Markoli, F. Zupanic, *J. Alloy. Compd.*, 505 (2010) p. 486.

1  
2  
3  
4  
5  
6  
7  
8  
9  
10  
11  
12  
13  
14  
15  
16  
17  
18  
19  
20  
21  
22  
23  
24  
25  
26  
27  
28  
29  
30  
31  
32  
33  
34  
35  
36  
37  
38  
39  
40  
41  
42  
43  
44  
45  
46  
47  
48  
49  
50  
51  
52  
53  
54  
55  
56  
57  
58  
59  
60

### Table captions

Table 1: Chemical composition of the alloys cast into a 1-mm copper die, determined using inductively coupled plasma – atomic emission spectroscopy

	Al <sub>94</sub> Mn <sub>3</sub> Cu <sub>3</sub>	Al <sub>96.5</sub> Mn <sub>1.3</sub> Cu <sub>1.6</sub> Be <sub>0.6</sub>	Al <sub>95.4</sub> Mn <sub>1.8</sub> Cu <sub>1.5</sub> Be <sub>1.3</sub>	Al <sub>92.4</sub> Mn <sub>4.4</sub> Cu <sub>1.6</sub> Be <sub>1.6</sub>
	at. %	at. %	at.	at. %
Mn	2.86	1.25	1.82	4.44
Cu	3.12	1.58	1.53	1.57
Be	0	0.62	1.24	1.58
Al	94.02	96.55	95.41	92.41
Mn/Cu	0.92	0.79	1.19	2.82
Be + Mn	2.85	1.87	3.06	6.02

Table 2: Microindentation properties (load 1 N) and Vickers hardness of alloys cast into a small copper-die in the as-cast (s – slow cooling, m – moderate cooling) conditions and in the annealed (a) condition.  $HM$  – Martens hardness,  $HV_{IT}$  – Vickers indentation hardness,  $E_r$  – reduced modulus,  $\eta_{IT}$  – fraction of the elastic energy,  $HV 1$  – Vickers hardness (load 10 N)

		$Al_{94}Mn_3Cu_3$	$Al_{96.5}Mn_{1.3}Cu_{1.6}Be_{0.6}$	$Al_{95.4}Mn_{1.8}Cu_{1.5}Be_{1.3}$	$Al_{92.4}Mn_{4.4}Cu_{1.6}Be_{1.6}$
$HM / GPa$	s	1.10	0.92	0.99	0.87
	m	1.18	1.08	1.20	1.43
	a	1.17	0.97	0.87	1.20
$HV_{IT} / GPa$	s	0.99	0.80	0.88	73.63
	m	1.10	0.98	1.12	1.37
	a	1.11	0.89	0.80	1.11
$E_r / GPa$	s	74.65	75.68	83.68	79.58
	m	75.99	79.05	73.20	81.48
	a	73.56	71.33	69.39	80.09
$\eta_{IT} / \%$	s	10.38	8.39	10.3	9.37
	m	13.06	11.39	13.6	15.26
	a	13.62	11.49	10.5	13.17
$HV 1 / GPa$	s	0.98	0.95	0.99	1.01
	m	1.13	1.10	1.17	1.60
	a	1.16	0.98	0.88	1.15

## Figure captions

Figure 1: Backscattered electron micrographs after vacuum induction melting and casting into a cylindrical 50-mm die: a)  $\text{Al}_{94}\text{Mn}_3\text{Cu}_3$  b)  $\text{Al}_{96.5}\text{Mn}_{1.3}\text{Cu}_{1.6}\text{Be}_{0.6}$ , c)  $\text{Al}_{95.4}\text{Mn}_{1.8}\text{Cu}_{1.5}\text{Be}_{1.3}$  and d)  $\text{Al}_{92.4}\text{Mn}_{4.4}\text{Cu}_{1.6}\text{Be}_{1.6}$ . Note that no  $\text{Al}_6\text{Mn}$  formed in the quaternary alloys, while the Be-rich phase  $\text{Be}_4\text{Al}(\text{Mn},\text{Cu})$  appeared in the interdendritic regions.

Figure 2: 2D-XRD after VIM for a)  $\text{Al}_{94}\text{Mn}_3\text{Cu}_3$  b)  $\text{Al}_{96.5}\text{Mn}_{1.3}\text{Cu}_{1.6}\text{Be}_{0.6}$ , c)  $\text{Al}_{95.4}\text{Mn}_{1.8}\text{Cu}_{1.5}\text{Be}_{1.3}$  and d)  $\text{Al}_{92.4}\text{Mn}_{4.4}\text{Cu}_{1.6}\text{Be}_{1.6}$ . Note that the heights of  $\tau_1$ - and  $\theta$ - $\text{Al}_2\text{Cu}$ -peaks considerably reduced in the quaternary alloys, but the heights of  $\text{Al}_4\text{Mn}$ -peaks increased. The peaks of  $\text{Be}_4\text{Al}(\text{Mn},\text{Cu})$  are hardly seen due to its very small volume fraction.

Figure 3: ToF SIMS mapping of Al-, Cu-, Be- and Mn-secondary ions in  $\text{Al}_{95.4}\text{Mn}_{1.8}\text{Cu}_{1.5}\text{Be}_{1.3}$  after slow cooling (few  $\text{K s}^{-1}$ ). Note that Be is present in all phases, yet its content is negligible in the  $\alpha$ -Al.

Figure 4: DSC-traces obtained at a cooling rate of  $20 \text{ K min}^{-1}$  for  $\text{Al}_{94}\text{Mn}_3\text{Cu}_3$ ,  $\text{Al}_{96.5}\text{Mn}_{1.3}\text{Cu}_{1.6}\text{Be}_{0.6}$ ,  $\text{Al}_{95.4}\text{Mn}_{1.8}\text{Cu}_{1.5}\text{Be}_{1.3}$  and  $\text{Al}_{92.4}\text{Mn}_{4.4}\text{Cu}_{1.6}\text{Be}_{1.6}$ . Peak 1: primary crystallization of  $\text{Al}_4\text{Mn}$ , peak 2: formation of  $\alpha$ -Al, and peak 3: terminal stage of solidification.

Figure 5: Microstructures of alloys after casting into a 1-mm die for a)  $\text{Al}_{94}\text{Mn}_3\text{Cu}_3$  b)  $\text{Al}_{96.5}\text{Mn}_{1.3}\text{Cu}_{1.6}\text{Be}_{0.6}$ , c)  $\text{Al}_{95.4}\text{Mn}_{1.8}\text{Cu}_{1.5}\text{Be}_{1.3}$  and d)  $\text{Al}_{92.4}\text{Mn}_{4.4}\text{Cu}_{1.6}\text{Be}_{1.6}$ . Approximate cooling rate was  $1000 \text{ K s}^{-1}$ . In the ternary alloy, primary  $\text{Al}_4\text{Mn}$  dominates, with very small fractions of  $\tau_1$  and  $\theta$ - $\text{Al}_2\text{Cu}$  in interdendritic spaces. In the quaternary alloy i-phase formed, but no  $\tau_1$ ,  $\text{Be}_4\text{Al}(\text{Mn},\text{Cu})$ ,  $\text{Al}_4\text{Mn}$  and  $\text{Al}_6\text{Mn}$ . Only in alloy  $\text{Al}_{92.4}\text{Mn}_{4.4}\text{Cu}_{1.6}\text{Be}_{1.6}$  was an additional phase (presumably  $\text{Al}_4\text{Mn}$ ) formed around the (i-phase +  $\alpha$ -Al) eutectic cells. In all alloys,  $\theta$ - $\text{Al}_2\text{Cu}$  formed during terminal stages of solidification.

Figure 6: XRD-traces for  $\text{Al}_{94}\text{Mn}_3\text{Cu}_3$ ,  $\text{Al}_{96.5}\text{Mn}_{1.3}\text{Cu}_{1.6}\text{Be}_{0.6}$ ,  $\text{Al}_{95.4}\text{Mn}_{1.8}\text{Cu}_{1.5}\text{Be}_{1.3}$  and d)  $\text{Al}_{92.4}\text{Mn}_{4.4}\text{Cu}_{1.6}\text{Be}_{1.6}$  after casting into a 1-mm copper die. Peaks of  $\theta$ - $\text{Al}_2\text{Cu}$ ,  $\text{Al}_4\text{Mn}$  and  $\alpha$ -Al are observed in the ternary alloy. In quaternary alloys in addition to  $\theta$ - $\text{Al}_2\text{Cu}$ , rather wide peaks belonging to i-phase appeared. Only in the  $\text{Al}_{92.4}\text{Mn}_{4.4}\text{Cu}_{1.6}\text{Be}_{1.6}$  alloy, also additional peaks presumably belonging to  $\text{Al}_4\text{Mn}$  can be seen.

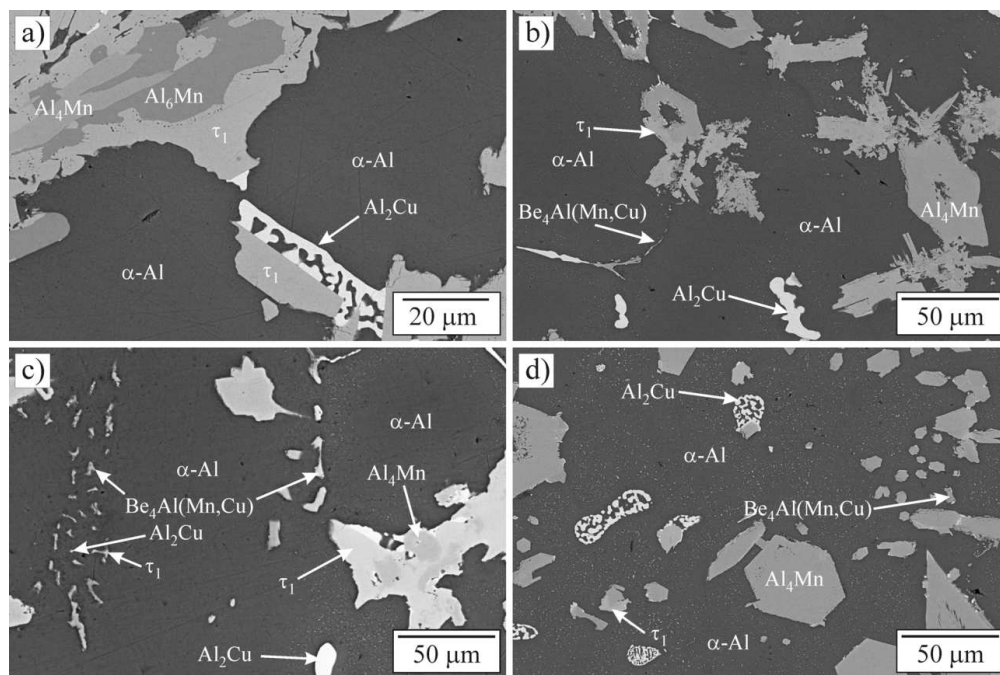
Figure 7: Icosahedral quasicrystalline phase as a part of binary i-phase and  $\alpha$ -Al eutectic. a) Bright-field transmission electron micrograph, and b) the corresponding selected area diffraction pattern taken along a fivefold axis.

Figure 8: ToF SIMS mapping of Al-, Cu-, Be- and Mn-secondary ions in  $\text{Al}_{95.4}\text{Mn}_{1.8}\text{Cu}_{1.5}\text{Be}_{1.3}$  after solidification in a small Cu-die (cooling rate  $\approx 1000 \text{ K s}^{-1}$ ). Note that Be is present in both the primary and eutectic i-phase.

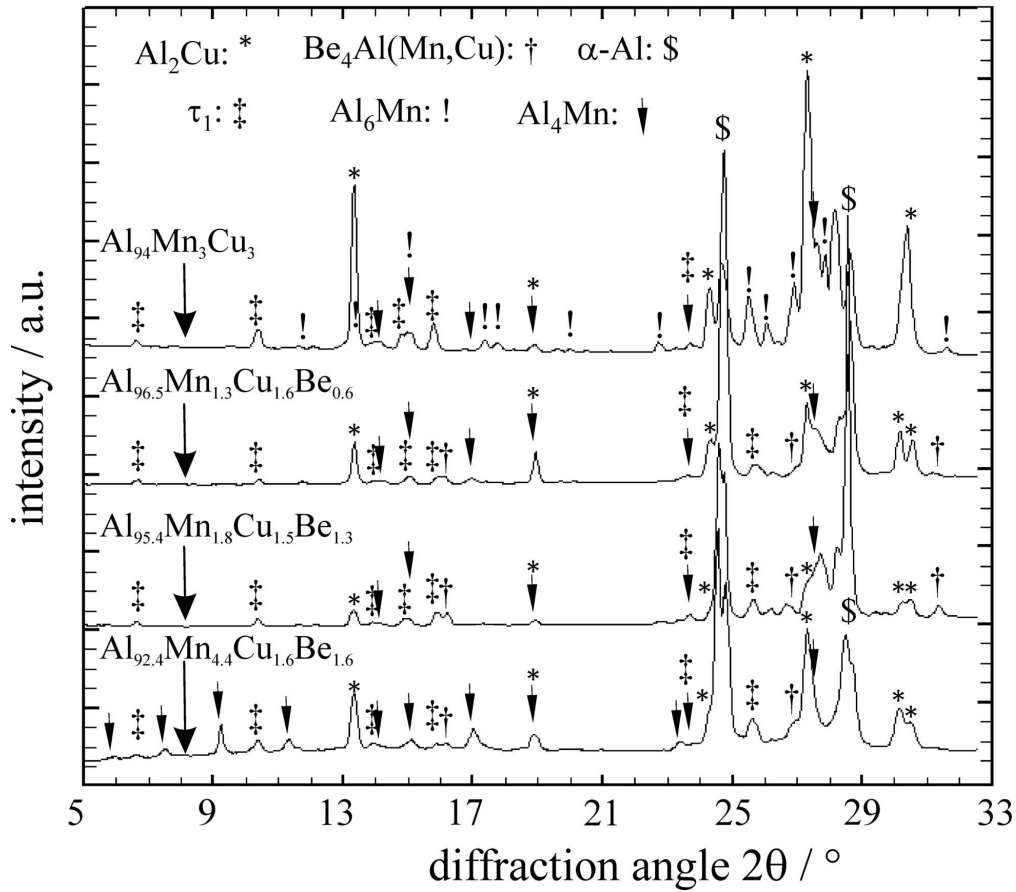
Figure 9: Heating curves for a)  $\text{Al}_{94}\text{Mn}_3\text{Cu}_3$  b)  $\text{Al}_{96.5}\text{Mn}_{1.3}\text{Cu}_{1.6}\text{Be}_{0.6}$ , c)  $\text{Al}_{95.4}\text{Mn}_{1.8}\text{Cu}_{1.5}\text{Be}_{1.3}$  and d)  $\text{Al}_{92.4}\text{Mn}_{4.4}\text{Cu}_{1.6}\text{Be}_{1.6}$

1  
2  
3 Figure 10: Backscattered electron micrographs of the alloys a)  $\text{Al}_{94}\text{Mn}_3\text{Cu}_3$  b)  
4  $\text{Al}_{96.5}\text{Mn}_{1.3}\text{Cu}_{1.6}\text{Be}_{0.6}$ , c)  $\text{Al}_{95.4}\text{Mn}_{1.8}\text{Cu}_{1.5}\text{Be}_{1.3}$  and d)  $\text{Al}_{92.4}\text{Mn}_{4.4}\text{Cu}_{1.6}\text{Be}_{1.6}$  annealing at  
5  $500^\circ\text{C}$  for 1 hour. In alloy  $\text{Al}_{94}\text{Mn}_3\text{Cu}_3$ ,  $\tau_1$  almost completely replaced  $\text{Al}_4\text{Mn}$ .  
6 Additional  $\tau_1$  precipitates formed in the  $\alpha$ -Al matrix.  $\theta$ - $\text{Al}_2\text{Cu}$  coagulated in rounded  
7 particles. In the quaternary alloys, rods of eutectic i-phase turned into particles, almost  
8 whole  $\theta$ - $\text{Al}_2\text{Cu}$  dissolved in the matrix, whilst in the matrix a high fraction of  
9 precipitates formed. Primary i-phase remained, however its surface became covered  
10 with  $\tau_1$  and  $\text{Be}_4\text{Al}(\text{Mn},\text{Cu})$ .  
11  
12  
13

14 Figure 11: XRD-traces of alloys a)  $\text{Al}_{94}\text{Mn}_3\text{Cu}_3$  b)  $\text{Al}_{96.5}\text{Mn}_{1.3}\text{Cu}_{1.6}\text{Be}_{0.6}$ , c)  
15  $\text{Al}_{95.4}\text{Mn}_{1.8}\text{Cu}_{1.5}\text{Be}_{1.3}$  and d)  $\text{Al}_{92.4}\text{Mn}_{4.4}\text{Cu}_{1.6}\text{Be}_{1.6}$  annealed at  $500^\circ\text{C}$  for 1 h. In all  
16 alloys the fractions of  $\tau_1$  increased considerably, whereas the fractions of  $\theta$ - $\text{Al}_2\text{Cu}$   
17 decreased. In the ternary alloy the  $\text{Al}_4\text{Mn}$ -peaks disappeared almost completely, whilst  
18 they were considerably reduced in the alloy  $\text{Al}_{92.4}\text{Mn}_{4.4}\text{Cu}_{1.6}\text{Be}_{1.6}$ . In all quaternary  
19 alloys i-phase remained, however its peaks start to overlap with those of  $\tau_1$ .  
20  
21  
22  
23  
24  
25  
26  
27  
28  
29  
30  
31  
32  
33  
34  
35  
36  
37  
38  
39  
40  
41  
42  
43  
44  
45  
46  
47  
48  
49  
50  
51  
52  
53  
54  
55  
56  
57  
58  
59  
60

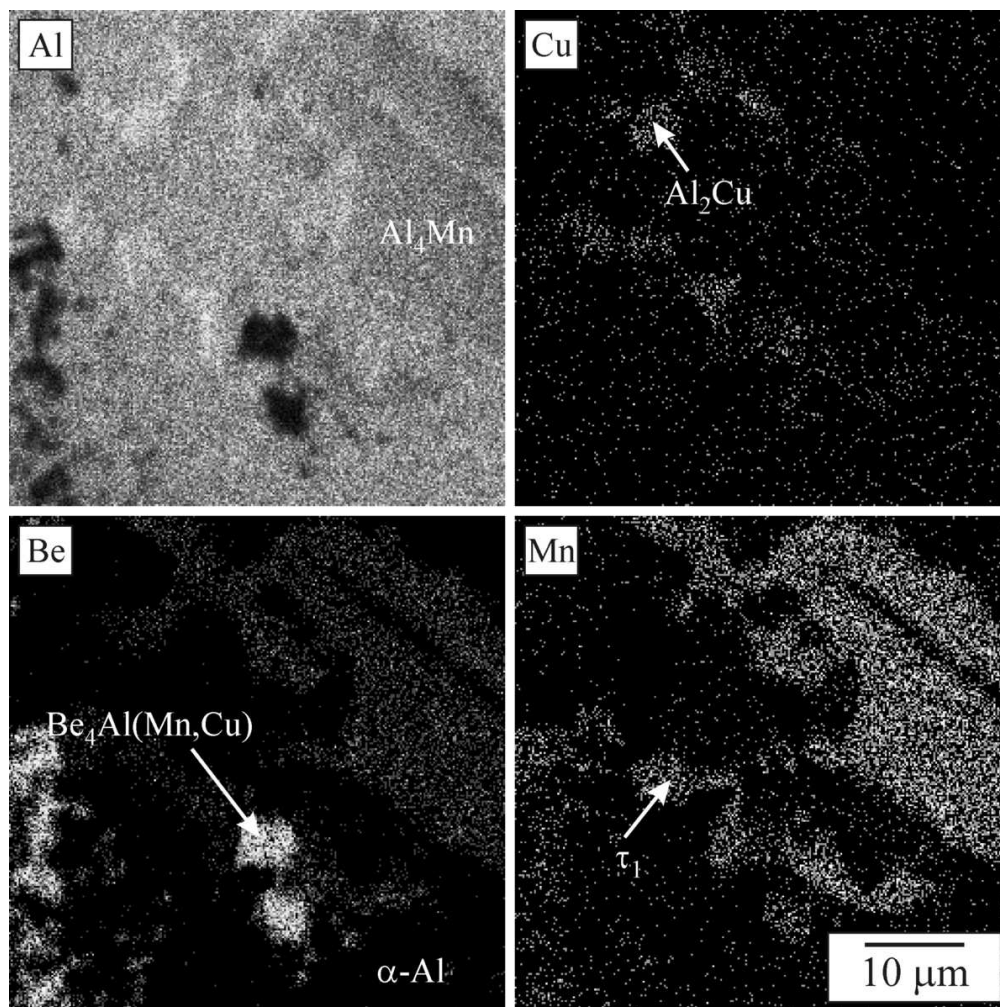


Microstructure after slow cooling  
a) Al-Mn-Cu, b-d) Al-Mn-Cu-Be alloys  
108x72mm (300 x 300 DPI)

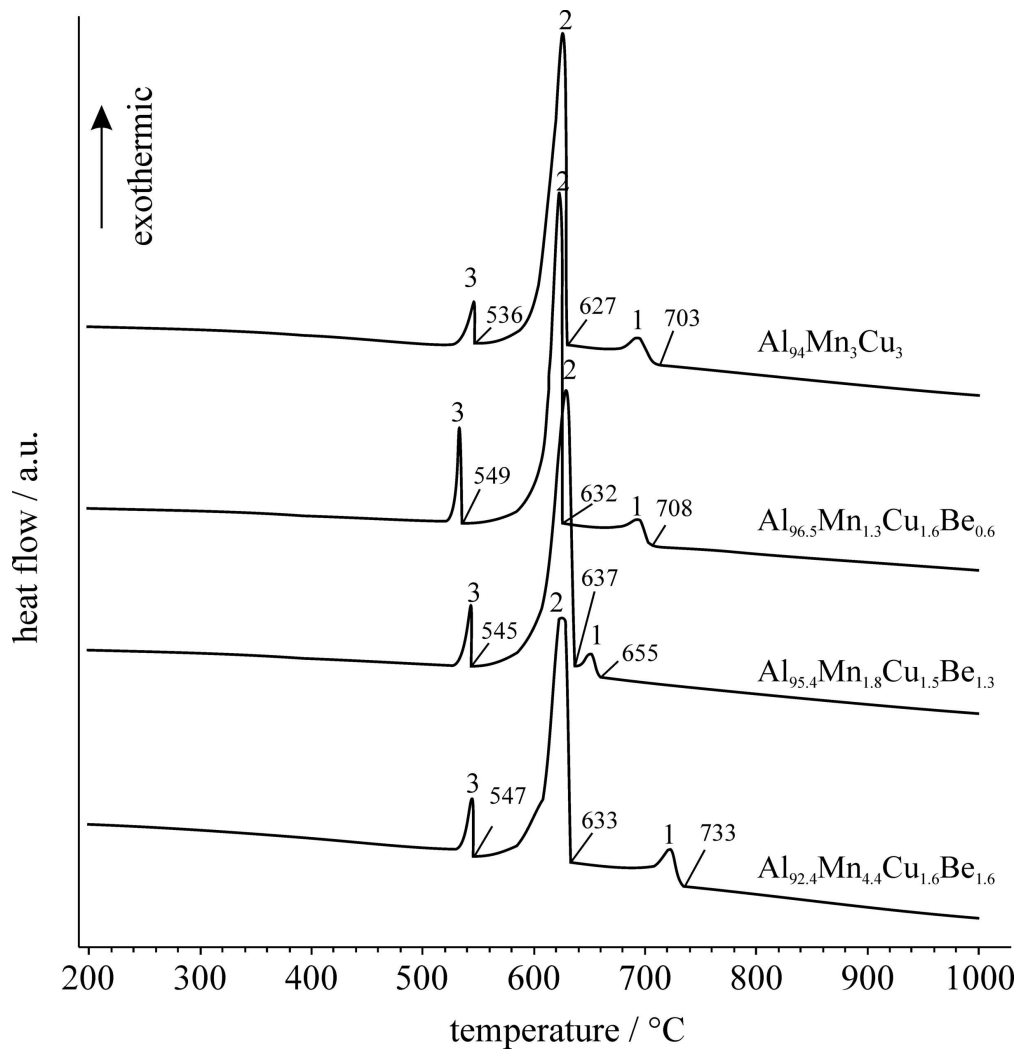


X-ray diffraction traces after slow cooling  
 82x73mm (600 x 600 DPI)

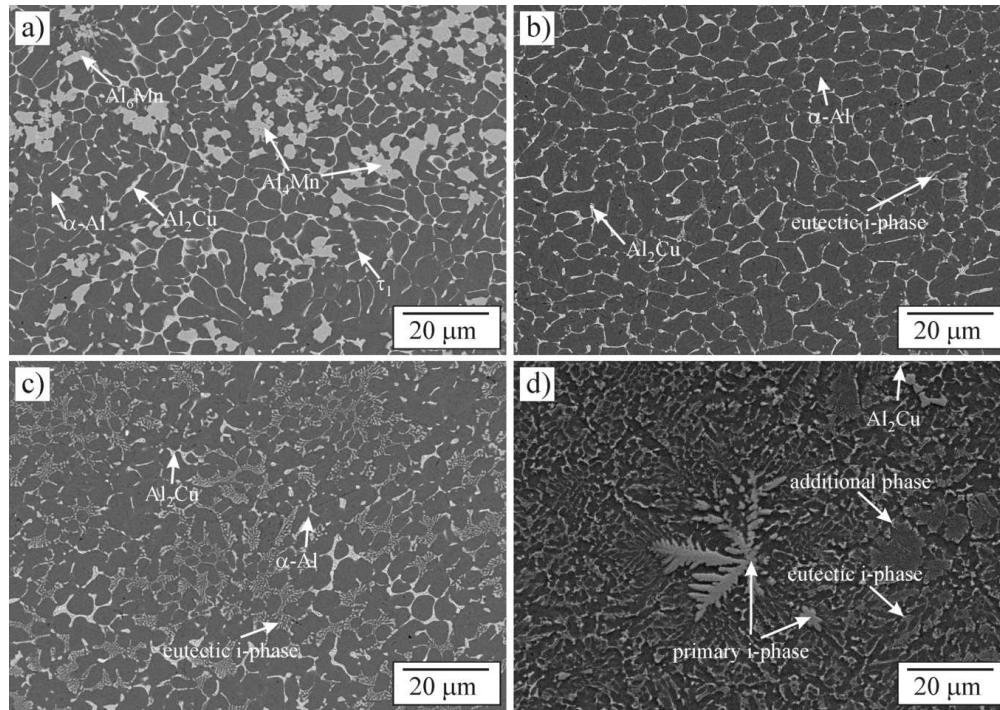
Only



Tof-SIMS mapping of a quaternary alloy after slow cooling  
100x100mm (300 x 300 DPI)

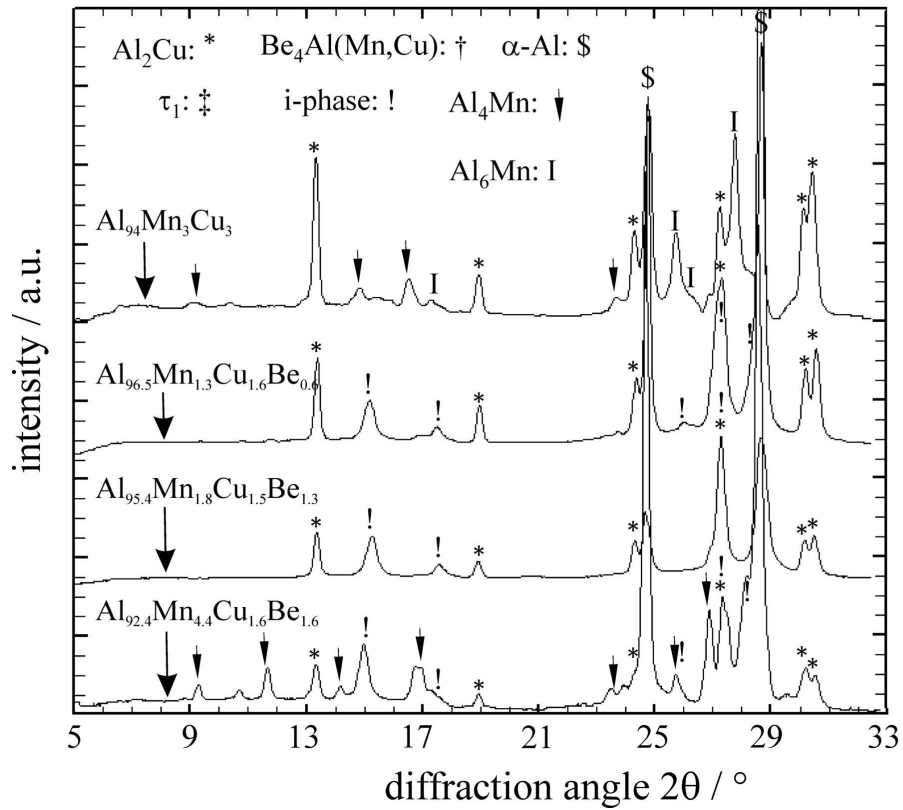


DSC cooling curves for Al-Mn-Cu and Al-Mn-Cu-Be alloys  
102x106mm (600 x 600 DPI)



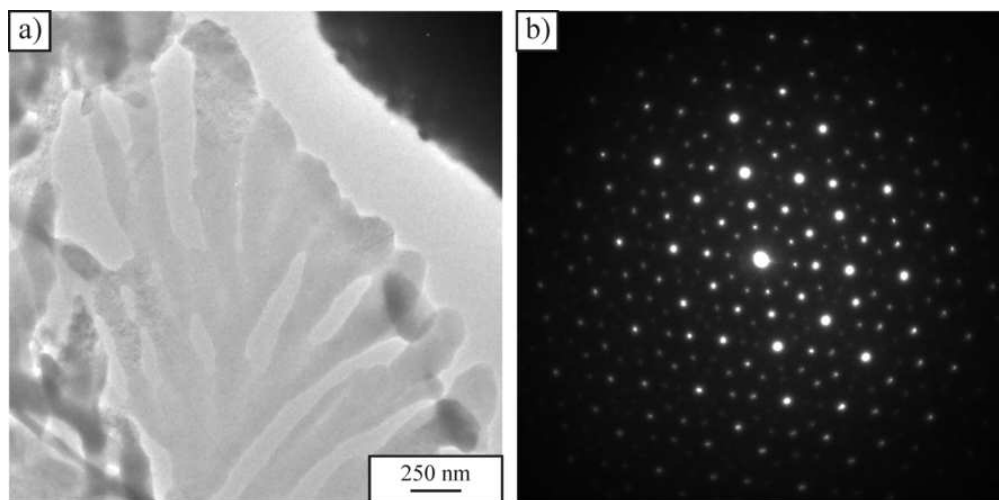
Microstructure of Al-Mn-Be and Al-Mn-Be-Cu alloys after moderate cooling  
114x80mm (300 x 300 DPI)

view Only



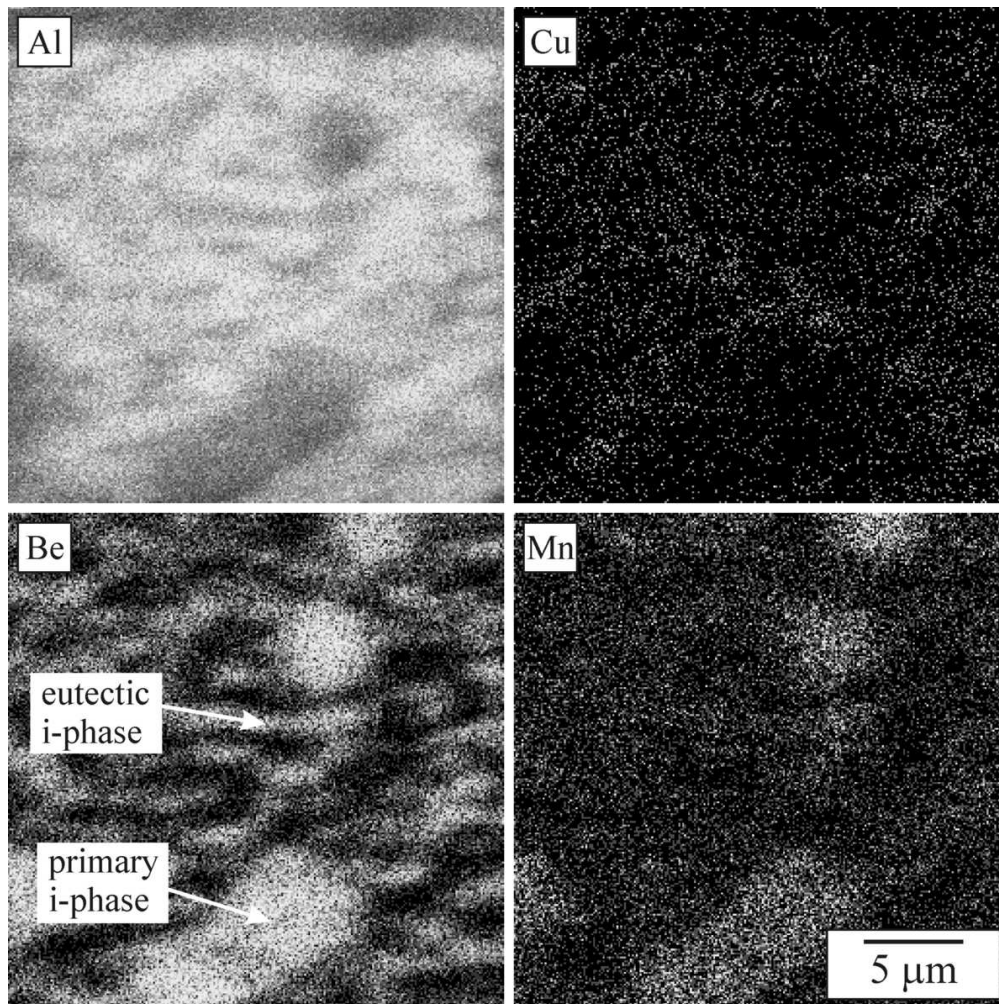
37

XRD traces for Al-Mn-Cu and Al-Mn-Cu-Be alloy after moderate cooling  
84x68mm (600 x 600 DPI)



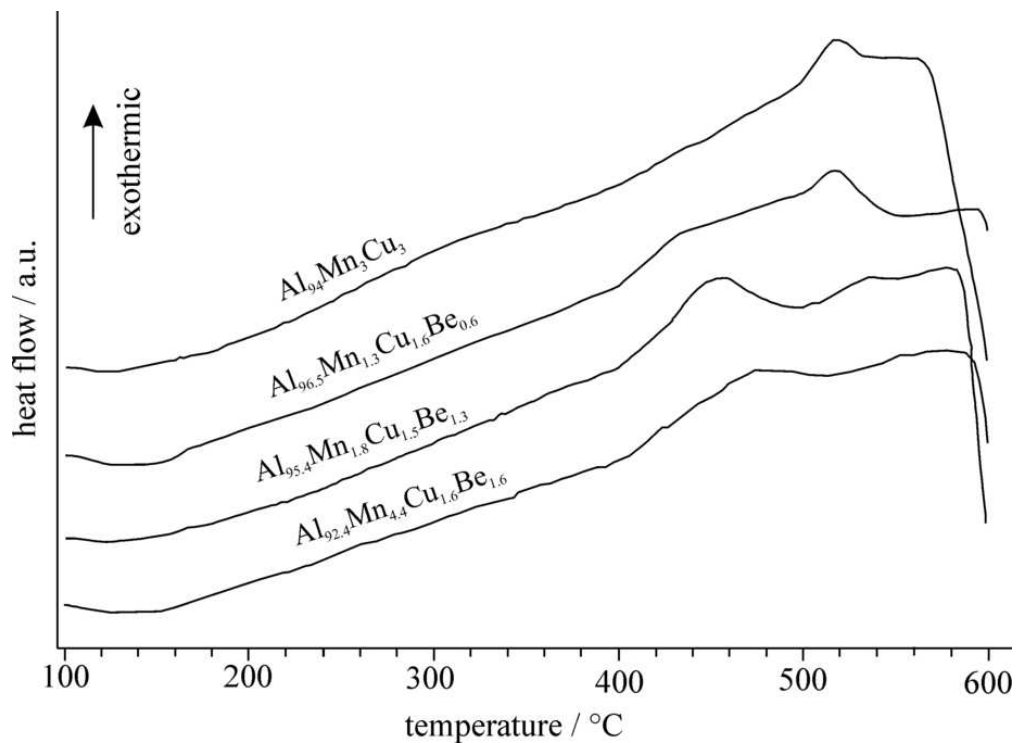
TEM micrograph of eutectic icosahedral phase and its fivefold diffraction pattern  
75x37mm (300 x 300 DPI)

1  
2  
3  
4  
5  
6  
7  
8  
9  
10  
11  
12  
13  
14  
15  
16  
17  
18  
19  
20  
21  
22  
23  
24  
25  
26  
27  
28  
29  
30  
31  
32  
33  
34  
35  
36  
37  
38  
39  
40  
41  
42  
43  
44  
45  
46  
47  
48  
49  
50  
51  
52  
53  
54  
55  
56  
57  
58  
59  
60

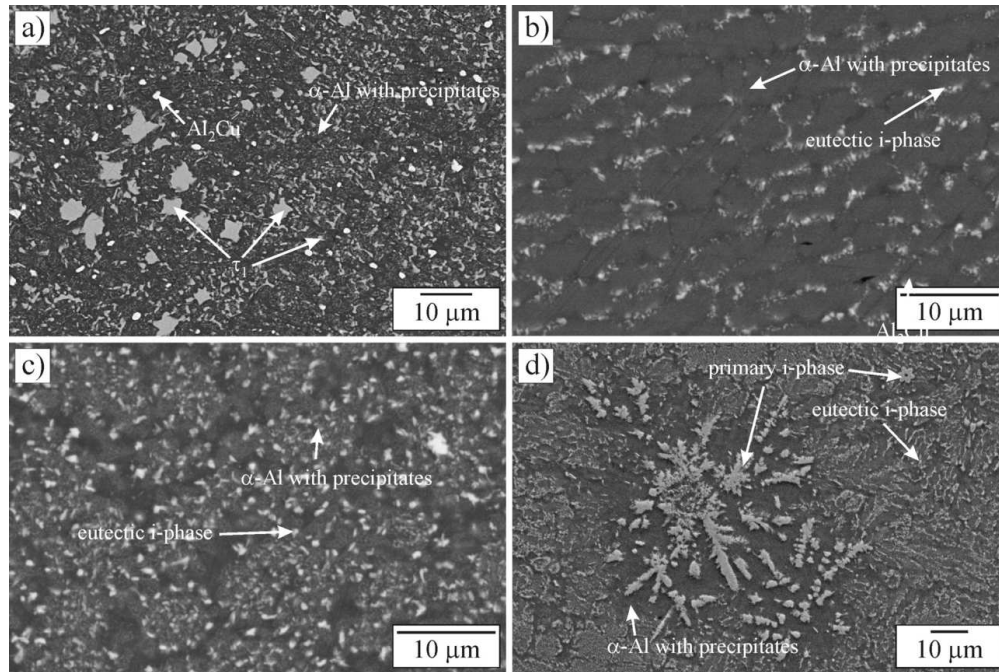


ToF SIMS mapping of the icosahedral phase in Al-Mn-Cu-Be alloy after moderate cooling  
100x100mm (300 x 300 DPI)

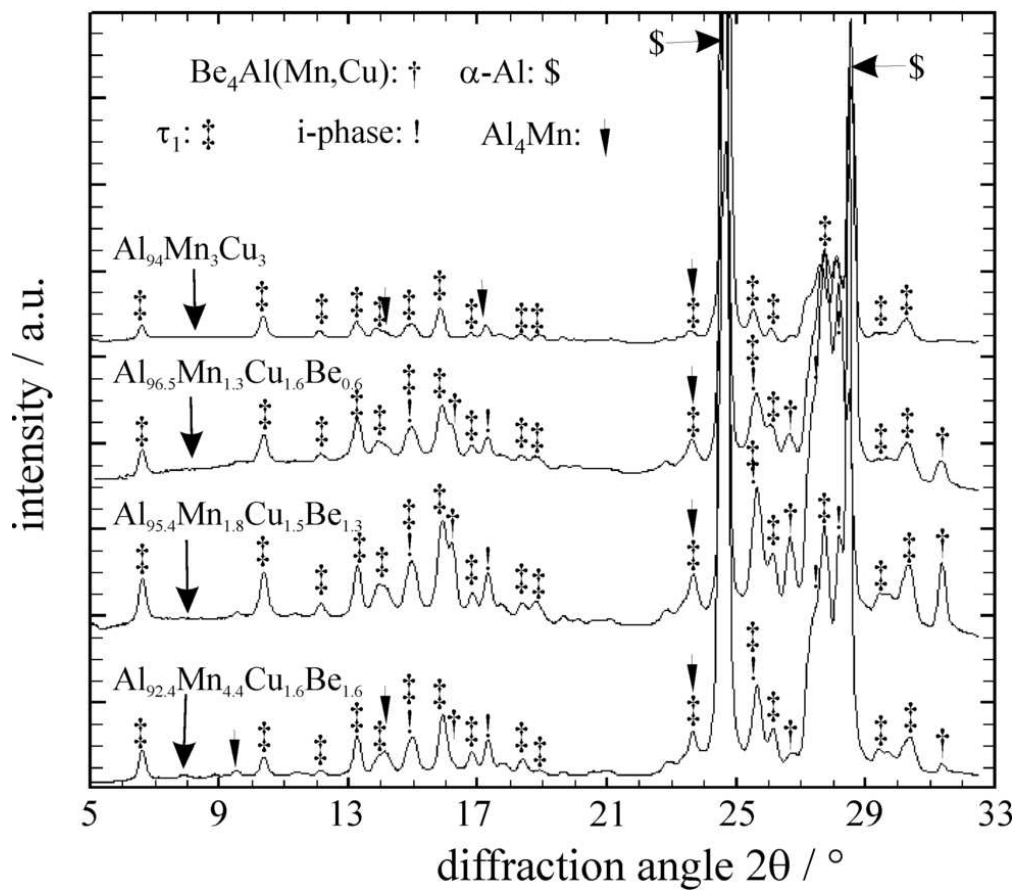
only



DSC heating curves, initial contion, moderately cooled samples  
77x57mm (300 x 300 DPI)



Microstructures after annealing moderately cooled samples, 500 deg C, 1 h  
108x72mm (300 x 300 DPI)



XRD traces after annealing for 1 h at 500 deg C  
 82x73mm (300 x 300 DPI)

	$\text{Al}_{94}\text{Mn}_3\text{Cu}_3$	$\text{Al}_{96.5}\text{Mn}_{1.3}\text{Cu}_{1.6}\text{Be}_{0.6}$	$\text{Al}_{95.4}\text{Mn}_{1.8}\text{Cu}_{1.5}\text{Be}_{1.3}$	$\text{Al}_{92.4}\text{Mn}_{4.4}\text{Cu}_{1.6}\text{Be}_{1.6}$
	at. %	at. %	at.	at. %
Mn	2.86	1.25	1.82	4.44
Cu	3.12	1.58	1.53	1.57
Be	0	0.62	1.24	1.58
Al	94.02	96.55	95.41	92.41
Mn/Cu	0.92	0.79	1.19	2.82
Be + Mn	2.85	1.87	3.06	6.02

For Peer Review Only

		$\text{Al}_{94}\text{Mn}_3\text{Cu}_3$	$\text{Al}_{96.5}\text{Mn}_{1.3}\text{Cu}_{1.6}\text{Be}_{0.6}$	$\text{Al}_{95.4}\text{Mn}_{1.8}\text{Cu}_{1.5}\text{Be}_{1.3}$	$\text{Al}_{92.4}\text{Mn}_{4.4}\text{Cu}_{1.6}\text{Be}_{1.6}$
$HM / \text{GPa}$	s	1.10	0.92	0.99	0.87
	c	1.18	1.08	1.20	1.43
	a	1.17	0.97	0.87	1.20
$HV_{IT} / \text{GPa}$	s	0.99	0.80	0.88	73.63
	c	1.10	0.98	1.12	1.37
	a	1.11	0.89	0.80	1.11
$E_r / \text{GPa}$	s	74.65	75.68	83.68	79.58
	c	75.99	79.05	73.20	81.48
	a	73.56	71.33	69.39	80.09
$\eta_{IT} / \%$	s	10.38	8.39	10.3	9.37
	c	13.06	11.39	13.6	15.26
	a	13.62	11.49	10.5	13.17
$HV 1 / \text{GPa}$	s	0.98	0.95	0.99	1.01
	c	1.13	1.10	1.17	1.60
	a	1.16	0.98	0.88	1.15